Available online at www.sciencedirect.com
SCIENCE DIRECT®
Journal of Organometallic Chemistry 690 (2005) 1511–1522
Journal of Organometallic Chemistry
www.elsevier.com/locate/jorganchem

# The cocondensation reaction of lithium atoms and anisole: an experimental and theoretical study of the reaction pathway

Oscar Mendoza, Laurence P. Cuffe, Franz-Josef K. Rehmann, Matthias Tacke *

*Department of Chemistry, Centre for Synthesis and Chemical Biology (CSCB), Conway Institute of Biomolecular and Biomedical Research, University College Dublin, Belfield, Dublin 4, Ireland*

Received 28 October 2004; accepted 17 December 2004
Available online 7 February 2005

**Abstract**

The cocondensation reaction of lithium atoms and pure anisole leads to an *ortho* CH activation and the formation of lithium hydride. This simple two-component system allows the investigation of the reaction mechanism with included donor molecules. Therefore two anisole and one dilithium molecule, which was identified in an earlier spectroscopic study, were considered for the reaction pathway calculations.

Firstly, two intermediates can be found along the reaction pathway, which show the reaction before and after the critical CH activation step. Secondly, a low-lying transition state can be identified, which allows the carbon hydrogen bond to be broken with an activation energy of less than 20 kcal/mol instead of more than 100 kcal/mol, if a free radical mechanism is employed. All calculations were performed at the B3LYP/6-31G** level of theory.


*Keywords:* Lithium atoms; Metal vapour synthesis; CH activation; Reaction pathway calculation; DFT

## 1. Introduction

The activation of carbon–hydrogen bonds has been a major topic of research for the last 30 years [1–3]. Earlier reports involving lithium atoms [4–6] showed that they are able to activate aromatic hydrocarbons in the presence of THF selectively under cocondensation conditions at 77 K. This resulted in the direct synthesis of aryl-lithium compounds on a synthetic scale.

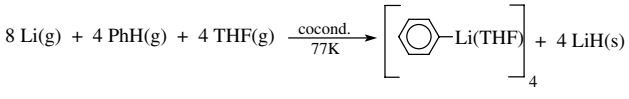


One of the key intermediates in this reaction is a $Li_2$–benzene π-complex. This complex is capable of undergoing a two-electron transfer from the $Li_2$ to the lowest unoccupied molecular orbital (LUMO) of the aromatic ring, resulting in the activation of the aromatic C–H bond.

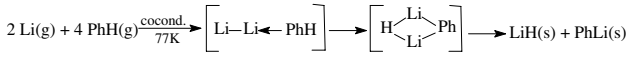


The work has been expanded to +I substituted ($CMe_3$, $SiMe_3$, *o*- and *m*-Xylene) and donor substituted (OMe, $NMe_2$, SMe) benzene derivatives recently [7]. In the case of anisole a selective C–H bond activation in the presence of THF was found to occur in the *ortho* position. The aim of this paper is to understand the reaction mechanism occurring in a cocondensation reaction of lithium atoms and pure anisole, when THF is not present.

* Corresponding author. Tel.: +353 17168428; fax: +353 17162127.
*E-mail address:* matthias.tacke@ucd.ie (M. Tacke).

0022-328X/$ - see front matter © 2004 Elsevier B.V. All rights reserved.
doi:10.1016/j.jorganchem.2004.12.016

## 2. Experimental study

Many aromatic compounds, as benzenes or heterocycles, show C–H activation when cocondensed with lithium atoms at 77 K. The presence of THF molecules was shown to be an essential part of the cocondensation reaction.

Previous studies showed the cocondensation reaction of lithium and −I substituted benzenes compounds, as anisole, in the presence of THF. For all the cases, the observed lithiated compound was shown to be *ortho* lithiated.

In this study the *ortho* position where the C–H activation occurs was blocked. For this propose the reactions of 2-methyl anisole and 2,6-dimethyl anisole were carried out under cocondensation conditions. Both showed two lithiated products from the cocondensation experiment: substituted phenyl lithium was found as a result of a C–H activation and lithium phenolate as a result of a C–O activation [8,9].

In the case of one *ortho* position blocked as in 2-methyl anisole, the C–H activation was found in the second *ortho* position. However for 2,6-dimethyl anisole the activation was found in the *para* position with respect to the methoxy group and it is shown in Scheme 1.

In order to study the importance of a donor solvent in these reactions, a cocondensation reaction of anisole and lithiums atoms was carried out without the presence of THF as additional oxygen donor ligand. Also a lithiated product was observed and identified as 2-lithio anisole (Scheme 2).

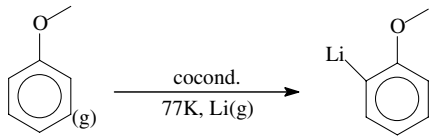


Scheme 2. Cocondensation reaction of lithium atoms with anisole at 77 K.

## 3. Theoretical study

Theoretical studies and thermodynamic details for organolithium species have been reported previously [10–13]. A simple example shows the reaction of benzene and its derivates with lithium atoms, which under cocondensation conditions are able to activate C–H bonds in the presence of THF [5]. The DFT study of the reactions showed reaction pathways where different intermediates were identified. The formation of a dilithium molecule and its interaction with the aromatic system of anisole has been the main topic.

As reported previously, the benzene derivate anisole shows a C–H activation reaction when cocondensed with lithium atoms without the involvement of THF as solvent. The aim of this work is to identify, by calculation, plausible intermediate species for the anisole cocondensation reaction of lithium atoms without THF, and thereby identifying the local minima and transition states in all the possible pathways. Calculations were performed using GAUSSIAN-98 [14] and the B3LYP DFT functional [15–18] in combination with the 6-31G** [19–22] basis set.

Initially, one anisole molecule interacting with the dilithium species was considered. The C–H activation involves several steps and several intermediates can be identified in this pathway reaction. Once the $Li_2$ species is formed from two lithium atoms, its coordination with the aromatic compound gives three possible first stable intermediates (**1a**–**c**) in exothermic reactions (Scheme 3). In this intermediate the dilithium molecule forms a complex with the anisole in three different ways: a σ-complex with the oxygen (**1b**), a π-complex with the aromatic ring (**1c**) and both σ- and π-complex at the same time (**1a**) (Scheme 3). The formation of **1a** could be considered as a direct formation from dilithium and anisole or through the formation of a previous intermediate **1b** or **1c**.

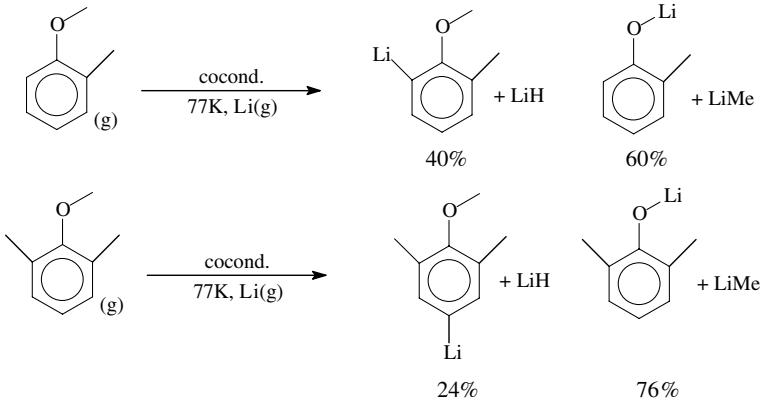


Scheme 1. Cocondensation reaction of lithium atoms with 2-methyl anisole and 2,6-dimethyl anisole at 77 K in presence of THF.

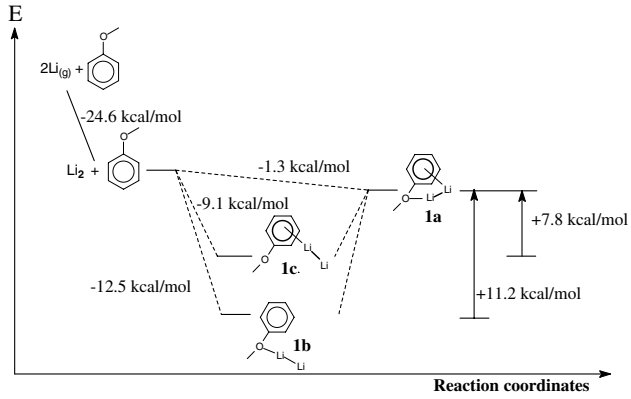


Scheme 3. Formation energies for the first three intermediates of the reaction.

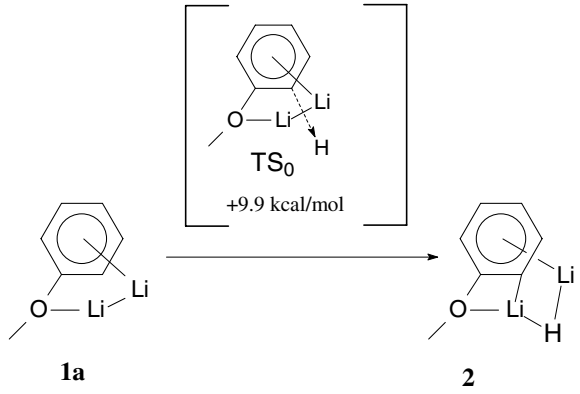


Scheme 4. C–H activation step in the pathway involving one anisole molecule.

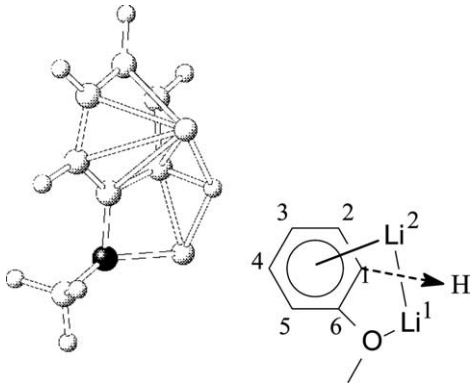


Fig. 1. Gaussview plot of the transition state $TS_0$ involving one anisole molecule.

The three first intermediate are stable structures and show a local minimum in energy. Formation involves exothermic reaction for all of them, however σ-coordination shows a more exothermic reaction enthalpy of −12.5 kcal/mol.

The reaction mechanism shows intermediates compounds optimised as a local minimum, however this is not an equilibrium reaction and the species have additional energy due to the high exothermic first step (formation of dilithium). This energy added to species **1b** could enable the presence of **1a**.

The next step on the reaction pathway is the activation of the C–H bond. As previously reported [7], this step involves the double electron transfer from the intermediate **1a**–**c** to the LUMO of the aromatic ring and this results in the insertion of the $Li_2$ into the C–H bond. The step involves an endothermic reaction step to reach a transition state, and then an exothermic process leads to a second intermediate **2**. For this purpose **1a** is considered as the first intermediate because it is so closely related to the structure of the calculated transition state. In order to reach the transition state from **1a**, the *ortho* C–H bond on the anisole molecule is elongated and moves through the lithium–lithium bond. The Li–Li distance widens as well and allows the formation of a C–$Li_2$–H four-membered ring in a third intermediate (Scheme 4).

On this pathway, the transition state ($TS_0$) identified shows only one negative frequency of $-513\ cm^{-1}$. This corresponds to the hydrogen moving across the lithium–lithium bond. Fig. 1 shows the numbering scheme that is used in Tables 1 and 2.

During this activation, an elongation on the C–H bond from 108.7 in **1a** to 298.6 pm in **2** occurs. In the transition state the C–H bond is widened to 137.5 pm (Table 1), while the Li–Li distance is elongated from 285.8 pm in **1a** to non-bonding 355.3 pm in the transition state (Table 2).

After the activation of the C–H bond leading to **2** one more intermediate (**3**) is found before the final product is formed. In this species the π-interaction of the ring with the second lithium disappears and a C–Li sigma bond is formed instead (Scheme 5). This is an exothermic step of −7.5 kcal/mol and leads to a structure characterised by the electron deficient C–$Li_2$–H ring.

The last step in this process is the formation of solid LiH and 2-lithio anisole, which is characterised by X-ray crystallography [23]. The solid-state structure of this compound consists of four lithium atoms arranged in a slightly distorted tetrahedron, which binds to the four anisyl groups. The anionic carbon atom of an anisyl group is bonded to three lithium atoms. An asymmetry of this structure comes from the fact that two lithium atoms have only one O–Li contact and the other two have either two or none (Fig. 2).

The most important distances of the crystal and calculated DFT structure are presented in Table 3. Both data sets show very similar bond length, only Li2–C12 and Li4–C42 show larger differences than 10 pm.

To carry out the calculation of the thermodynamical data of the last step, two considerations are necessary. All the calculations and thermodynamical values have been calculated at B3LYP/6-31G** level, however the

Table 1
Selected bond distances and negative frequency of the calculated structure of the transition state ($TS_0$)

| $TS_0$ | (pm) |
|---|---|
| C(1)–Li(2) | 220.3 |
| C(2)–Li(2) | 217.8 |
| C(3)–Li(2) | 216.4 |
| C(4)–Li(2) | 220.7 |
| C(5)–Li(2) | 243.0 |
| C(6)–Li(2) | 242.7 |
| C(1)–Li(1) | 194.5 |
| C(1)–H | 137.5 |
| *v* | $-513\ cm^{-1}$ |

Table 2
Selected interatomic distances for the calculated structures of **1a**, $TS_0$ and **2**

| | **1a** (pm) | $TS_0$ (pm) | **2** (pm) |
|---|---|---|---|
| C(1)–H | 108.7 | 137.5 | 298.6 |
| Li(1)–Li(2) | 285.8 | 355.3 | 260.1 |
| O–Li(1) | 201.6 | 196.5 | 209.3 |
| Li(1)–C(1) | 227.9 | 194.5 | 207.3 |
| Li(2)–C(1) | 225.2 | 220.3 | 228.5 |

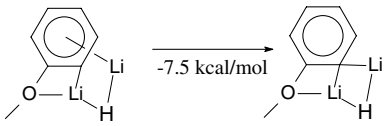


**2** **3**

Scheme 5. Formation of intermediate 3 in a reaction involving one anisole molecule.

vibrational energies for the tetrameric lithium anisole structure was computed at B3LYP/3-21G* level of theory. Experimental values were included for the formation of solid LiH and the $Li_2$ molecule (Scheme 6).

The electron deficient $Li_2$ molecule will accept electron density from the aromatic anisole to form an expected σ-complex **1b** or unusual π-complex **1c**. The next mechanistic step is crucial and involves the double electron transfer from the lithium complex to the LUMO of the aromatic ring.

Studies of the charge distribution in $TS_0$ and **1a** were carried out and are presented in Table 4. Intermediate **1a** shows a small positive charge (0.12 au) on the Li–Li while a negative is found on the aromatic ring. The electronic distribution probe that the dilithium is already transferring electrons to the aromatic system occupying the LUMO of the ring. The calculated structure **1a** shows a negligible difference in energy when calculated in a triplet or singlet state and makes them both possible intermediates.

After the formation of (**1a**–**c**) by exothermic reaction steps, the activation of the CH bond occurs and leads to **2** through the transition state. The charge distribution

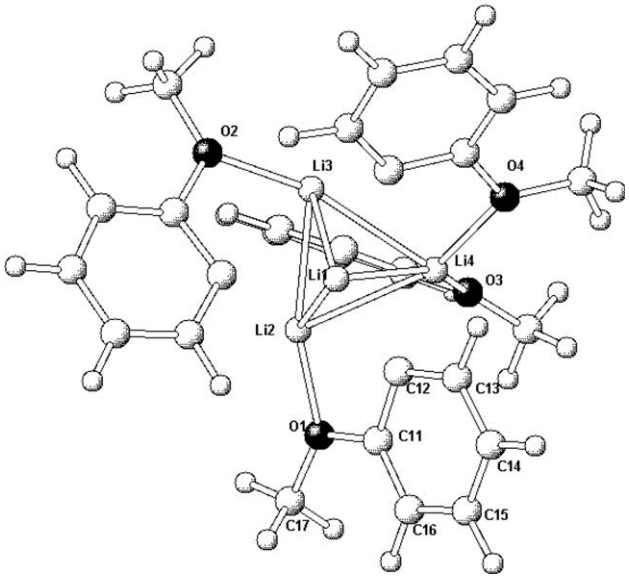


Fig. 2. Gaussview plot of tetrameric 2-lithio anisole (Li–C bonds have been omitted for clarity).

Table 3
Selected bond distances for tetrameric 2-lithio anisole from the crystal and the DFT structure

| | Bond length (pm) crystal structure | Bond length (pm) DFT calculation |
|---|---|---|
| Li(1)–C(22) | 218 | 218.0 |
| Li(1)–C(12) | 221 | 216.4 |
| Li(1)–C(42) | 223 | 216.1 |
| Li(2)–O(1) | 193 | 193.7 |
| Li(2)–C(12) | 225 | 243.6 |
| Li(2)–C(22) | 220 | 220.1 |
| Li(2)–C(32) | 213 | 220.4 |
| Li(3)–O(2) | 195 | 196.0 |
| Li(3)–C(22) | 244 | 245.8 |
| Li(3)–C(32) | 219 | 222.6 |
| Li(3)–C(42) | 222 | 219.9 |
| Li(4)–O(3) | 193 | 196.1 |
| Li(4)–O(4) | 201 | 196.4 |
| Li(4)–C(12) | 226 | 224.9 |
| Li(4)–C(32) | 251 | 244.3 |
| Li(4)–C(42) | 240 | 262.9 |
| Li(1)–Li(2) | 250 | 250.9 |
| Li(1)–Li(3) | 259 | 250.8 |
| Li(1)–Li(4) | 262 | 263.6 |
| Li(2)–Li(3) | 260 | 256.2 |
| Li(2)–Li(4) | 265 | 268.0 |
| Li(3)–Li(4) | 265 | 265.6 |

on $TS_0$ shows a larger positive charge on both lithium atoms and also a larger negative charge on the anisole molecule, which is distributed between the aromatic ring and the methoxy group.

When a second molecule of anisole is considered, the situation turns out to be more complicated and more pathways must be considered. The formation of the dilithium species followed by the coordination with one

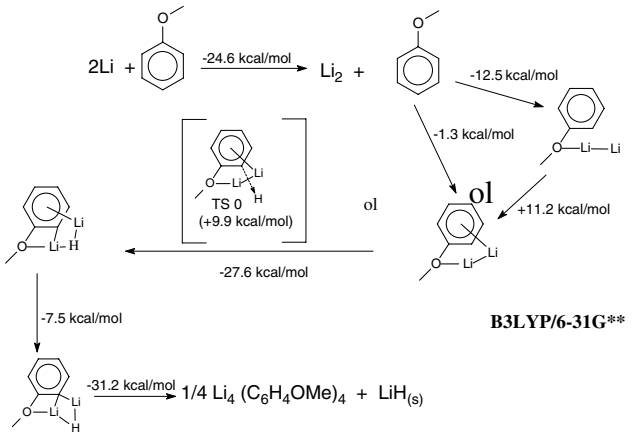


Scheme 6. Reaction pathway involving one anisole molecule and two lithium atoms.

Table 4
Charge distribution for the structure of **1a** and $TS_0$

| | **1a** | $TS_0$ |
|---|---|---|
| Li(1) | +0.019 | +0.654 |
| Li(2) | +0.103 | +0.415 |
| O | +0.048 | −0.502 |
| C(1) | −0.463 | −0.774 |
| C(2) | +0.047 | +0.274 |
| C(3) | +0.226 | −0.092 |
| C(4) | −0.360 | −0.372 |
| C(5) | −0.064 | −0.288 |
| C(6) | +0.011 | +0.335 |

anisole molecule is found as well. However, at this point the second anisole molecule is coordinated to the Li–Li–anisole intermediate. For this purpose the structure element represented by **1b** and a further anisole molecule are considered to form a new intermediate.

Once one anisole molecule is coordinated to the dilithium species, the interaction with the second anisole takes place. Four different possibilities are found for this interaction: two possibilities arise from σ- or π-coordination with one lithium in the dilithium species, and the other two are formed from σ- or π-coordination with the other lithium. Scheme 7 shows the most stable first intermediates for the four different pathways.

### 3.1. Pathways 1 and 2

When a second anisole donor is forming a σ-complex, two pathways can be considered (pathways 1 and 2). A necessary first intermediate would be formed by the dilithium molecule σ- and π-bonded with one anisole (**1a**) and the other anisole molecule σ-coordinated to one of the two lithium atoms (**4a** and **6a**) as shown in Scheme 8.

Both species are found to be stable intermediates and their formations involve an exothermic step of −11.7 and −12.3 kcal/mol respectively, when synthesised from **1a** and one anisole molecule.

However, the necessary intermediates **4a** and **6a** could be formed via **4b** and **6b** respectively due to their stability (Scheme 8). Once the σ-complex **1b** is formed, the second anisole makes a new σ-coordination (**4b** and **6b**). Then the lithium–lithium bond approaches the aromatic ring. The aryl structure and one lithium coordinate and a π-complex are formed (**4a** and **6a**). This is an endothermic reaction step and needs 8.6 or 5.4 kcal/mol respectively; the result is presented in Scheme 9. However as explained on one anisole mechanism, this is not an equilibrium reaction and the species could have extra energy and would not be in a local minimum.

The next step is the activation of the C–H bond. For this reaction step the C–H bond elongates when it approaches the Li–Li bond, which is stretched as well while the hydrogen crosses the bond. Both transition states ($TS_1$, $TS_2$) have been characterised by one negative frequency only (−589 and −728 $cm^{-1}$ respectively) and show the hydrogen moving across the Li–Li bond and the lithium atoms. Their structural data are available from Table 5, while the calculated structures are presented in Fig. 3.

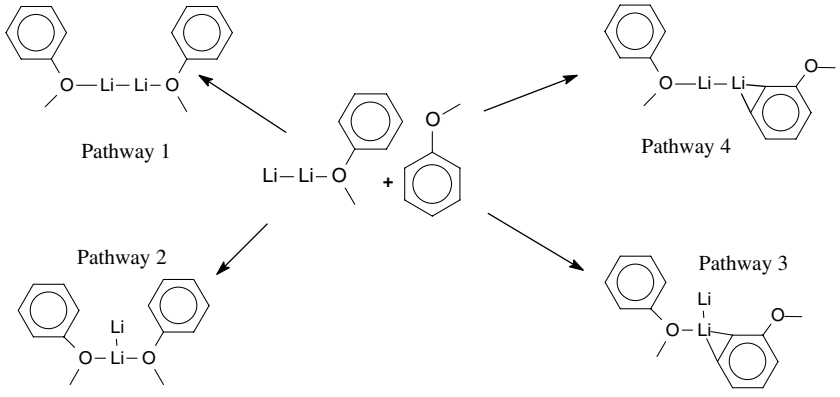


Scheme 7. Formation of most stable first intermediate when a second anisole molecule is considered.

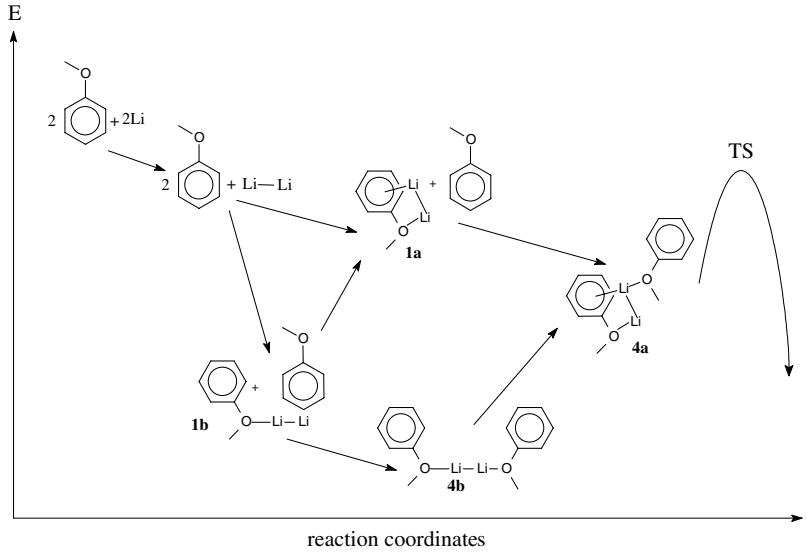


Scheme 8. Possible reaction steps for pathway 1 before reaching the transition state.

The π-coordination after the activation is only stable on pathway 2 (**7**), as Scheme 9 shows. For pathway 1 a second intermediate with a π-interaction is not found (see Tables 6 and 7).

The last step before the formation of 2-lithio anisole and lithium hydride, involves a final intermediate. As in one anisole pathway, the anisole lithium π-interaction disappears and a C–Li bond is found instead.

### 3.2. Pathway 3

When the second anisole involved has an π-interaction with **1a**, two new possibilities have been studied (pathways 3 and 4).

On pathway 3, as illustrated in Scheme 10, the π-interaction involves the lithium, which is already bonded to the oxygen, and the aromatic ring from the second anisole. However, the new π-system formed involves only one aromatic carbon (C1) instead of a total coordination with the six atoms ring (Fig. 4). These C–Li bonds are kept in all intermediates and the TS (Table 8). The numbering scheme and bonding details are shown in Fig. 4.

The route followed by the anisole molecules is similar than it was found on the two paths previously reported. The first intermediate is formed by the moiety **1a** and the second bonded anisole, followed by a transition state, in which frequency calculation shows the hydrogen moving through the Li–Li bond (Fig. 5). The intermediate **9a** can be formed via **1b** as described previously on pathways (Scheme 10).

As on pathway 2, a second intermediate (**10**) is found after the transition state, where the π-interaction involving the whole ring and Li2 is still seen. This is followed by the last stable intermediate (**11**), in which Li2 approaches C1 and does not coordinate with any other carbon. Structural data are presented in Table 9.

### 3.3. Pathway 4

The last pathway studied conferred a special case. The intermediate with lowest energy **12b** show the second anisole π-bonded with Li(2) where, as in path 3, two C–Li bonds characterise this coordination.

The configuration of **12a** is characterised by the position of the electron pair that is transferred from $Li_2$ to the aromatic ring during the C–H activation. A notably different structure can be observed when the electrons are still paired (singlet configuration) or when one electron from the Li–Li bond has been moved already (triplet).

The singlet configuration presents an expected anisole molecule double bounded with a dilithium species, while the second anisole has two C–Li bonds with Li(2) (Scheme 11). However this is not the stable configuration.

The calculated triplet structure has a negligibly lower energy of −0.5 kcal/mol, in which the two lithium atoms do not appear to be bonded (Li–Li: 395.1 pm) and the second anisole shows a clear π-interaction.

The TS (Table 5) for the C–H activation step also shows a singlet structure. The Li(2)–H does not appear bonded (278.6 pm) and the second anisole molecule shows a π-interaction (Fig. 6). The frequency calculation shows one negative vibration at $-429\ cm^{-1}$ where the hydrogen approach to the Li(1). While previously C–H bonds were elongated on pathway 4 the C–H bond is bent in order to cross the Li–Li bond.

As Scheme 10 shows, the final intermediate before the product is found on a stable single state. In **13** the

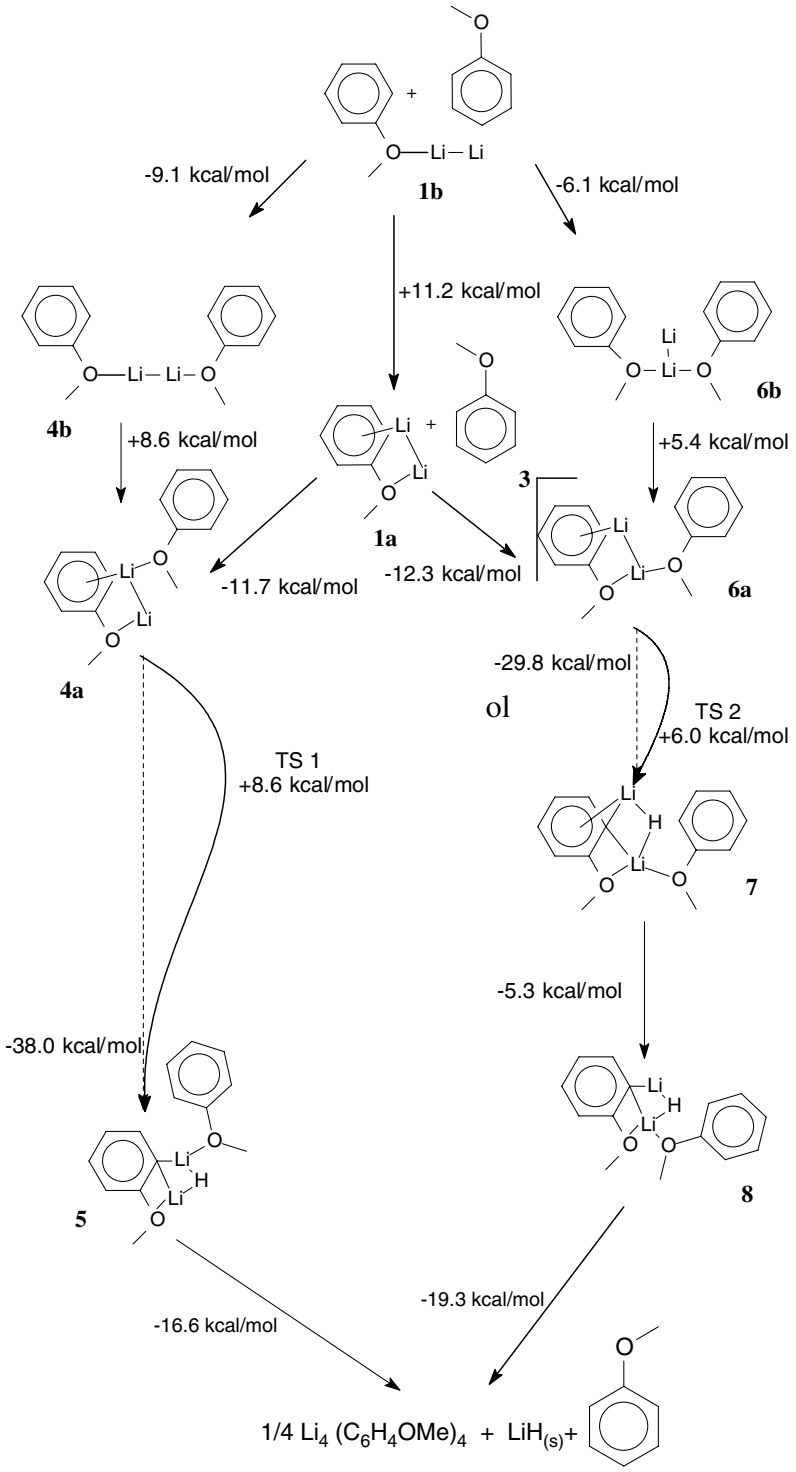


Scheme 9. Summary of the reactions pathways 1 and 2, when two anisole molecules are considered.

second anisole appears mainly bonded with three carbons in *para* and *meta* position with respect to the methoxy substituent (Table 10).

All the pathways converge in the final product. In the last step, lithium hydride and 2-lithio anisole are formed and the second anisole is liberated (see Table 11).

## 4. Discussion

The theoretical study of the cocondensation reaction of anisole and lithium atoms without the presence of further solvent molecules reveals four possible pathways. All these reaction pathways lead

Table 5
Selected bond distances and negative frequencies for transition states on pathways 1–4

| | $TS_1$ (pm) | $TS_2$ (pm) | $TS_3$ (pm) | $TS_4$ (pm) |
|---|---|---|---|---|
| C(1)–Li(2) | 228.0 | 219.6 | 218.8 | 238.4 |
| C(2)–Li(2) | 218.7 | 217.7 | 218.0 | 231.4 |
| C(3)–Li(2) | 217.7 | 217.0 | 218.1 | 226.7 |
| C(4)–Li(2) | 226.3 | 222.3 | 223.0 | 224.7 |
| C(5)–Li(2) | 249.5 | 244.5 | 242.2 | 236.6 |
| C(6)–Li(2) | 249.3 | 243.5 | 240.0 | 239.5 |
| $\nu$ ($cm^{-1}$) | −582.3 | −727.9 | −794.6 | −429.0 |

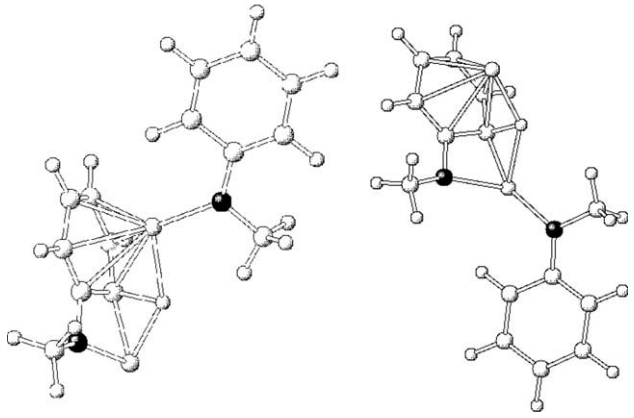

Fig. 3. Gaussview plot of the transition state structures for pathways 1–2.

Table 6
Selected interatomic distances for **4a**, **5** and $TS_1$ calculated structures on pathway 1

| | **4a** (pm) | $TS_1$ (pm) | **5** (pm) |
|---|---|---|---|
| C(1)–H | 108.6 | 138.9 | 321.5 |
| Li–Li | 292.3 | 363.7 | 232.6 |
| O–Li(1) | 202.1 | 197.5 | 190.7 |
| Li(1)–C | 231.4 | 193.8 | 223.4 |
| Li(2)–C | 229.3 | 228.0 | 216.3 |

Table 7
Selected interatomic distances for **6a**, **7**, **8** and $TS_2$ on pathway 2

| | **6a** (pm) | $TS_2$ (pm) | **7** (pm) | **8** (pm) |
|---|---|---|---|---|
| C(1)–H | 108.9 | 142.4 | 301.2 | 323.8 |
| Li(1)–Li(2) | 281.4 | 359.7 | 264.9 | 253.2 |
| O–Li(1) | 206.5 | 200.7 | 220.3 | 197.9 |
| Li(1)–C(1) | 229.9 | 197.6 | 211.4 | 239.6 |
| Li(2)–C(1) | 248.0 | 219.6 | 228.4 | 209.0 |

from lithium atoms and anisole molecules to the products 2-lithio anisole and lithium hydride via several intermediates.

In the case of one anisole, there is a clear pathway reaction through three intermediates. The formation energies show that all the steps can be exothermic except the formation of the transition state during the C–H activation step. This C–H activation step needs to cross through a transition state structure, which involves 9.9 kcal/mol to activate **1a**.

When the second anisole is considered, four different pathways are found. The first intermediate that can be considered occurs when the structure anisole–Li–Li (**1a**) coordinates with a second anisole molecule and lead **4a**, **6a**, **9a** and **12a**. As Fig. 7 shows, there is a moiety common in all the intermediates -a-, which is characterised by the dilithium molecule double bonded by σ- and π-coordination with the oxygen and the aromatic ring. This moiety (**1a**) was identified before on the pathway involving one anisole molecule. For all the cases, the formation of this intermediate can be considered via σ-complex -b-. All the first intermediates involve exothermic reactions.

The formation of **4**, **6**, **9** and **12a**, as a direct formation or via -b- intermediates, is necessary on all the cases due to -a- structures are the closest stable systems to the TS found. The formation of **4**, **6**, **9** and **12a** via -b- intermediates leads σ-complexes with better stability and high exothermic steps, however involves an endothermic step between b and a structures in all the cases. These b-intermediates were optimised as local minima, however the reaction pathway is not an equilibrium reaction and the b-intermediates have an additional energy due to the high exothermic first step (formation of dilithium). This could supply the formation of a-intermediates via b-intermediates.

During the reaction the $Li_2$ molecule will transfer two electrons to the aromatic ring. This electron movement can be found already on the structures immediately before the transition state. On these structures the electronic positions are not clearly distributed. A small energy barrier between singlet and triplet calculations shows that the electron pair is partially transferred. While pathway 1 shows less molecular energy on a singlet calculation, there is an opposite stability on pathways 2–4.

Immediately after the formation of intermediates **4**, **6**, **9** and **12a**, the C–H activation is observed. In pathways 1–3 the TS observed on this step show a similar behaviour: only one negative frequency where the hydrogen is moving across the Li–Li bond while Li–Li distance is elongated.

However in pathway 4, there is no interaction between the hydrogen and Li(2), and the negative frequency shows the hydrogen bending and approaching to Li(1).

The relative energies of a number of different reaction pathways can be compared. Scheme 12 shows relative energies for the most plausible reaction pathways studied leading to the final product. For each intermediate step on a given reaction pathway only the most stable isomer was chosen where a number of similar isomers were found.

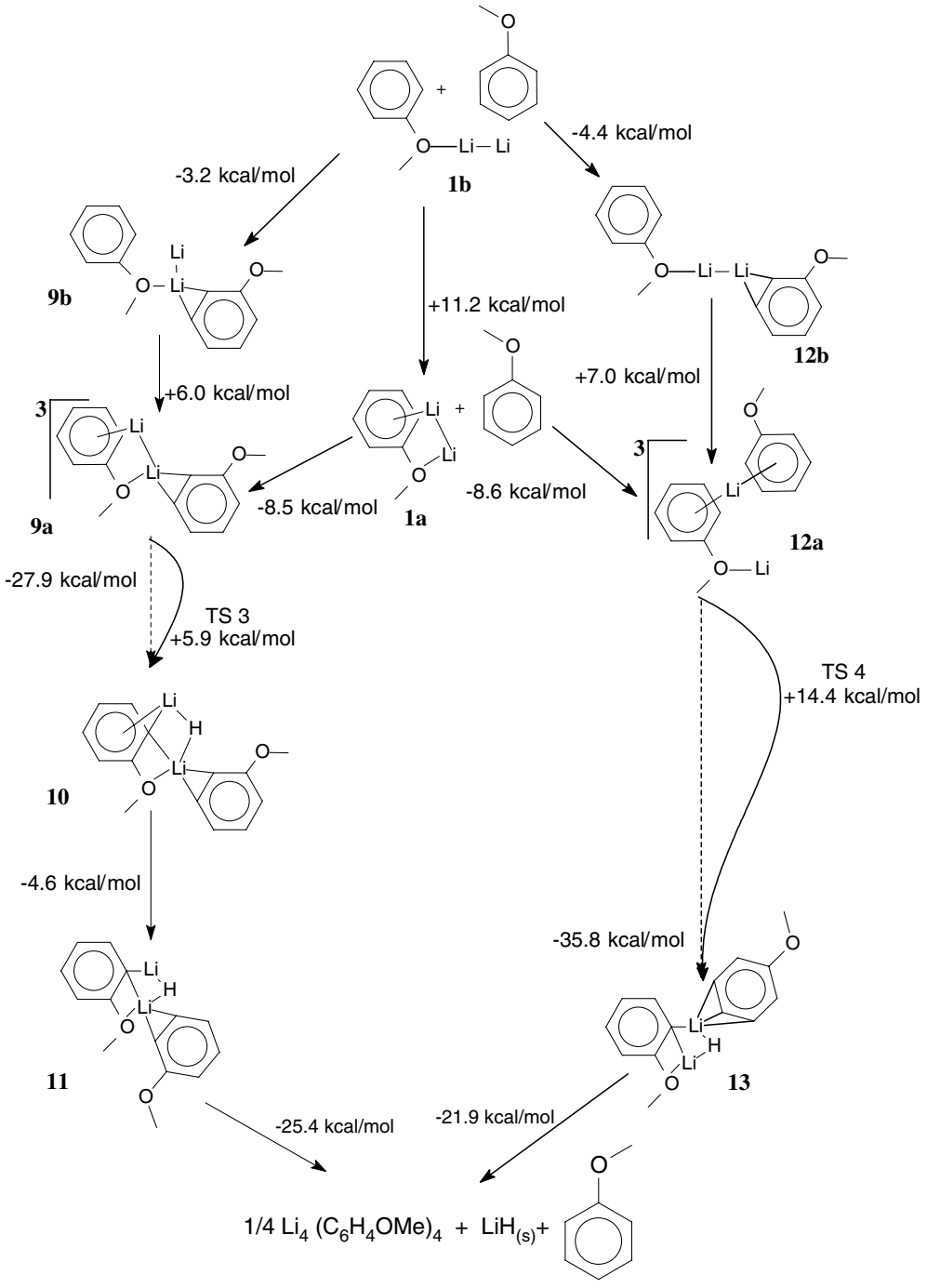


Scheme 10. Summary of the reactions pathways 1 and 2, when two anisole molecules are considered.

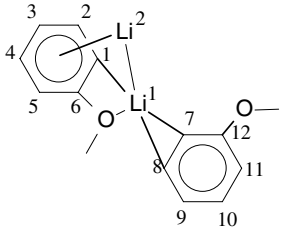

Fig. 4. Schematic structure of intermediate **9a**.

Table 8
Selected interatomic distances for **9a**, $TS_3$, **10** and **11** on pathway 3

| | **9a** (pm) | $TS_3$ (pm) | **10** (pm) | **11** (pm) |
|---|---|---|---|---|
| C(7)–Li(1) | 238.2 | 241.1 | 245.3 | 250.2 |
| C(8)–Li(1) | 240.6 | 241.0 | 264.9 | 275.4 |
| C(9)–Li(1) | 293.4 | 283.2 | 329.4 | 338.5 |
| C(10)–Li(1) | 337.5 | 320.4 | 369.5 | 372.5 |
| C(11)–Li(1) | 338.4 | 321.8 | 356.4 | 355.0 |
| C(12)–Li(1) | 293.3 | 284.7 | 297.9 | 296.8 |

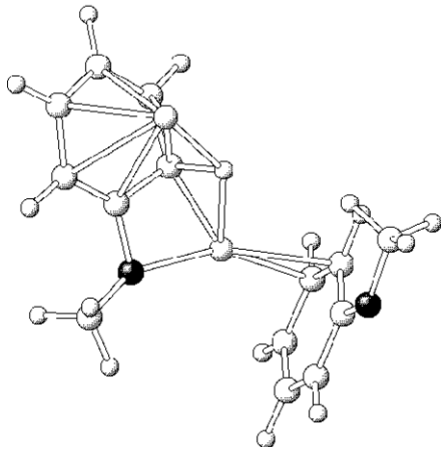

Fig. 5. Gaussview plot of the transition state structure on pathway 3.

Table 9
Selected interatomic distances for **9a**, **10**, **11** and $TS_3$ calculated structures on pathway 3

| | **9a** (pm) | $TS_3$ (pm) | **10** (pm) | **11** (pm) |
|---|---|---|---|---|
| C(1)–H | 109.0 | 144.2 | 298.7 | 323.7 |
| Li(1)–Li(2) | 285.9 | 359.0 | 267.1 | 236.3 |
| O–Li(1) | 202.5 | 201.6 | 210.7 | 194.9 |
| Li(1)–C(1) | 229.1 | 198.3 | 211.4 | 244.0 |
| Li(2)–C(1) | 245.1 | 218.8 | 226.0 | 208.3 |

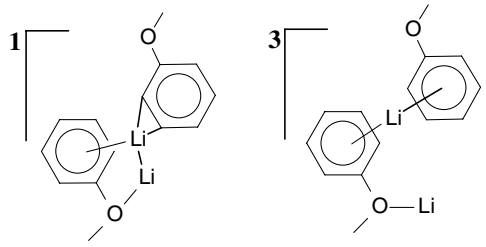


Scheme 11. Calculated structures for **12a** in singlet and triplet states.

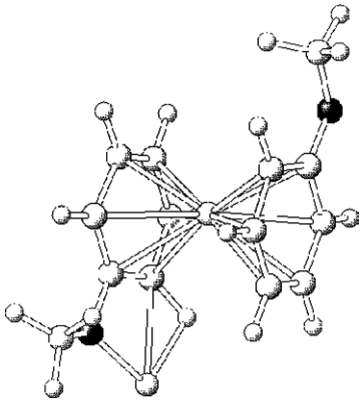

Fig. 6. Gaussview plot of the transition state structure on pathway 4.

Table 10
Selected interatomic distances for $^1$**12a**, $^3$**12a**, **13** and $TS_4$ calculated structures on pathway 4

| | $^1$**12a** | $^3$**12a** | $TS_4$ | **13** |
|---|---|---|---|---|
| C(7)–Li(2) | 233.3 | 240.9 | 239.2 | 305.1 |
| C(8)–Li(2) | 238.5 | 238.8 | 245.2 | 270.0 |
| C(9)–Li(2) | 302.6 | 240.0 | 249.4 | 249.8 |
| C(10)–Li(2) | 349.4 | 241.1 | 245.0 | 267.5 |
| C(11)–Li(2) | 344.0 | 244.2 | 236.2 | 303.5 |
| C(12)–Li(2) | 292.0 | 246.3 | 236.9 | 321.3 |

Table 11
Selected interatomic distances for $^3$**12a**, **13** and $TS_4$ calculated structures on pathway 4

| | $^3$**12a** (pm) | $TS_4$ (pm) | **13** (pm) |
|---|---|---|---|
| C(1)–H | 108.4 | 112.5 | 321.0 |
| Li–Li | 395.1 | 390.7 | 233.6 |
| O–Li(1) | 194.1 | 190.2 | 191.0 |
| Li(1)–C | 311.7 | 231.9 | 222.6 |
| Li(2)–C | 236.0 | 238.4 | 219.4 |

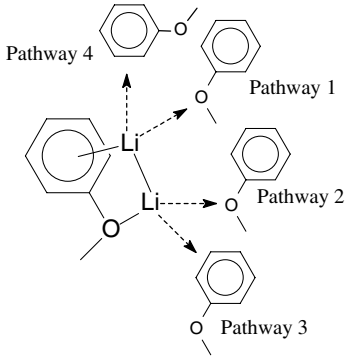


Fig. 7. General scheme of the interaction between moiety **1a** and the second anisole occurring on all studied pathways.

The reaction pathway involving a single anisole only is the least stable. For this pathway all reaction intermediates including the TS are higher in energy than the corresponding step on any pathway involving two anisole molecules.

When the second anisole molecule is considered and it is found to have a σ-coordination with the moiety **1a** or **1b** on pathways 1 and 2, the reaction takes place through more stable intermediates and transition states. Pathways 3 and 4 with π-interactions show higher energetic structures in all the cases. However, pathways 1 and 2 show very similar energies for all the steps, which are only separated by less than 3 kcal/mol.

When the intermediate activation energies are considered, that is the energy to reach the TS from a prior intermediate (**4a**, **6a**, **9a** and **12a**), pathways 1–3 require similar activation energy of 8.6, 6.0 and 5.9 kcal/mol, respectively. However, a significantly higher activation energy of 14.4 kcal/mol is found on pathway 4.

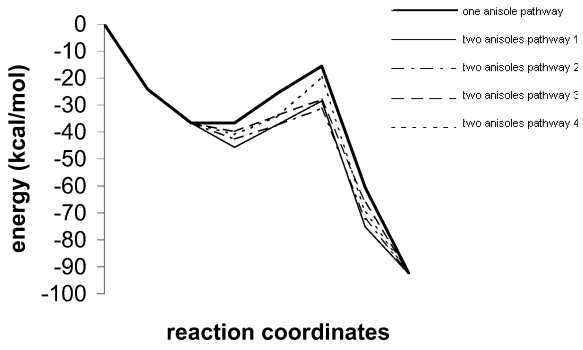


Scheme 12. Thermodynamical evolution for all studied pathways.

## 5. Conclusions

The cocondensation reaction of lithium atoms and anisole in the presence of THF leads to an *ortho* CH activation and the formation of lithium hydride. However this is not the only position that can be activated in anisole compounds. When methyl groups are placed in the *ortho* positions a C–H activation in the *para* position is found as well.

Lithium atoms and anisole in the absence of a solvent react under cocondensation conditions. A theoretical study of four possible reaction pathways reveals some common steps. The formation of a lithium–lithium bond, the interaction of this species with the anisole molecule and the formation of a transition state, in which the hydrogen is crossing the dilithium species, are the main steps in all the four reaction pathways.

The activation energy required for the CH activation in cocondensation reactions is clearly lower than that required by other techniques. The existence of low energy transition states in these systems is supported by theoretical studies of a simple system formed by one anisole molecule and two lithium atoms. When a second anisole is considered, while the reaction paths accessible to the system are more complex, the energies found are lower in all the cases. The presence of a second anisole stabilises the intermediate structures and results in reactions with a more accessible reaction path by lowering the activation energy in the critical step.

## 6. Experimental section

### 6.1. General

All experimental procedures were performed using standard Schlenk techniques under an atmosphere of dry argon. THF was dried and distilled from sodium benzophenone ketyl under an atmosphere of argon. Anisole, 2-methyl anisole and 2,4-dimethyl anisole were dried and distilled from calcium dihydride under an atmosphere of argon. All solvents were then degassed by three freeze–pump–thaw cycles. Celite was stored in an oven at 120 °C overnight and was dried under oil pump vacuum for 3 h before use. For each filtration a plug of approximately 6 cm of celite was used and each filtration was performed under the vigorous exclusion of air and moisture. $^{1}H$ and $^{13}C$ NMR spectra were obtained using either a Varian 300 MHz or a Varian 500 MHz NMR machine. All chemical shifts are reported in ppm and are reference to TMS. All GC MS samples were run as liquid samples in ethylacetate using a Finnigan Trace GC MS, equipped with a RTX-5MS 15 m column.

### 6.2. A typical cocondensation experiment

0.53 g (0.076 mol) of lithium metal was vapourised from an alumina crucible protected by a stainless-steel inlet at around 800 °C over 90 min and cocondensed with a mixture of 15 ml of the aromatic compound and 80 ml (1.12 mol) of THF. The solution was filtered over celite in order to remove the solid lithium hydride by-product and unreacted lithium metal. After removal of the solvent mixture in vacuo, a solid was isolated and washed with 20 ml of THF. The lithiated aromatic compound was identified by derivatisation with $Me_3SiCl$.

### 6.3. A typical derivatisation of the lithiated aromatic with $Me_3SiCl$

To a room temperature solution of 0.25 g of the lithiated aromatic in 20 ml of THF, $Me_3SiCl$ was added dropwise with vigorous stirring. The reaction was judged finished when a colour-change from dark red–yellow to pale yellow occurred. To this solution, 10 ml of water was added and the organic phase separated and the aqueous phase washed three times by 10 ml of dichloromethane. The combined organic extracts were dried over $MgSO_4$ and then the solvent was removed under reduced pressure, affording the derivative. GC MS, $^{1}H$ and $^{13}C$ NMR spectra were used to identify the products.

### 6.4. Theoretical methods used in this study

DFT calculations were performed using B3LYP and the 6-31G** basis set for C, H, O and Li. For this purpose the program GAUSSIAN-98 was used on a Dell workstation running Red Hat Linux. Harmonic vibrational frequencies, calculated at the same level, characterised stationary points and gave the zero-point energy. The difference in the sum of the electronic and the zero-point energies were interpreted as reaction enthalpies at 0 K. Charge distributions were obtained from geometry optimised structures using B3LYP/6-31G**.

### 6.5. 2-Methyl-6-trimethylsilyl anisole

The general procedure applied to 2-methyl anisole gave 6-lithio-2-methyl anisole (yellow solid) in 65% yield, which was identified as its TMS derivative: 1H NMR ($CDCl_3$) $\delta = 0.44$ ppm (s), $\delta = 2.35$ ppm (s), $\delta = 3.78$ ppm (s), $\delta = 7.05$ ppm (d, $J = 7.32$), $\delta = 7.22$ ppm (d, $J = 7.32$), $\delta = 7.28$ ppm (d, $J = 7.32$); 13C NMR ($CDCl_3$) $\delta = 1.4$, 16.8, 56.4, 121.7, 125.3, 126.5, 131.1, 134.7, 165.5 ppm.

### 6.6. 2,6-Dimethyl-4-trimethylsilyl anisole

The general procedure applied to 2-methyl anisole gave 4-lithio-2,6-dimethyl anisole (yellow solid) in 58% yield, which was identified as its TMS derivative: 1H NMR ($CDCl_3$) $\delta = 0.32$ ppm (s), $\delta = 2.27$ ppm (s), $\delta = 3.71$ ppm (s), $\delta = 7.02$ ppm (s); 13C NMR ($CDCl_3$) $\delta = 2.3$, 15.1, 58.6, 122.6, 126.2, 126.8, 156.0 ppm.

## Appendix A. Supplementary data

Supplementary data associated with this article can be found, in the online version at doi:10.1016/j.jorganchem.2004.12.016.

## References

[1] A.E. Shilov, G.B. Shul'pin, Chem. Rev. 97 (8) (1997) 2905.
[2] B.A. Arndtsen, R.G. Bergmann, T.A. Mobley, T.H. Petersen, Acc. Chem. Res. 28 (1995) 154.
[3] R.H. Crabtree, Chem. Rev. 95 (1995) 987.
[4] M. Tacke, Chem. Ber. 128 (1995) 91.
[5] M. Tacke, Chem. Ber. 129 (1996) 1369.
[6] M. Tacke, Eur. J. Inorg. Chem. (1998) 537.
[7] J.P. Dunne, M. Bockmeyer, M. Tacke, Eur. J. Inorg. Chem. (2003) 458.
[8] M. Taddei, A. Ricci, Synthesis (1986) 633.
[9] H. Yasuda, Y. Nakayama, K. Takei, A. Nakamura, Y. Kai, N. Kanehisa, J. Organomet. Chem. 473 (1994) 105.
[10] A.-M. Sapse, P. von Rague Schleyer (Eds.), Lithium Chemistry: A Theoretical Overview, Wiley, New York, 1995.
[11] M. Tacke, Chem. Ber. 128 (1995) 1051.
[12] M. Tacke, P. Sparrer, R. Teuber, H.-J. Stadter, F. Schuster, J. Mol. Struct. 349 (1995) 251.
[13] M. Tacke, R. Leyden, L.P. Cuffe, J. Mol. Struct. Theochem. 684 (2004) 211.
[14] M.J. Frisch, G.W. Trucks, H.B. Schlegel, G.E. Scuseria, M.A. Robb, J.R. Cheeseman, V.G. Zakrzewski, J.A. Montgomery Jr., R.E. Stratmann, J.C. Burant, S. Dapprich, J.M. Millam, A.D. Daniels, K.N. Kudin, M.C. Strain, O. Farkas, J. Tomasi, V. Barone, M. Cossi, R. Cammi, B. Mennucci, C. Pomelli, C. Adamo, S. Clifford, J. Ochterski, G.A. Petersson, P.Y. Ayala, Q. Cui, K. Morokuma, D.K. Malick, A.D. Rabuck, K. Raghavachari, J.B. Foresman, J. Cioslowski, J.V. Ortiz, A.G. Baboul, B.B. Stefanov, G. Liu, A. Liashenko, P. Piskorz, I. Komaromi, R. Gomperts, R.L. Martin, D.J. Fox, T. Keith, M.A. Al-Laham, C.Y. Peng, A. Nanayakkara, C. Gonzalez, M. Challacombe, P.M.W. Gill, B. Johnson, W. Chen, M.W. Wong, J.L. Andres, C. Gonzalez, M. Head-Gordon, E.S. Replogle, J.A. Pople, GAUSSIAN-98, Revision A.7, Gaussian Inc., Pittsburgh, PA, 1998.
[15] A.D. Becke, Phys. Rev. A 38 (1988) 3098.
[16] A.D. Becke, J. Chem. Phys. 98 (1993) 5648.
[17] C. Lee, W. Yang, R.G. Parr, Phys. Rev. B 37 (1988) 785.
[18] B. Miehlich, A. Savin, H. Stoll, H. Preuss, Chem. Phys. Lett. 157 (1989) 200.
[19] R. Ditchfield, W.J. Hehre, J.A. Pople, J. Chem. Phys. 54 (1971) 724.
[20] W.J. Hehre, J.A. Pople, J. Chem. Phys. 56 (1972) 4233.
[21] W.J. Hehre, W.A. Lathan, J. Chem. Phys. 56 (1972) 5255.
[22] W.J. Hehre, R. Ditchfield, J.A. Pople, J. Chem. Phys. 56 (1972) 2257.
[23] S. Harder, J. Boersma, L. Brandsma, G.P.M. van Mier, J. Kanters, J. Organomet. Chem. 364 (1989) 1.